Scaling description of the structure factor of fractal soot composites

C. M. Sorensen and C. Oh
Condensed Matter Laboratory, Department of Physics, Kansas State University, Manhattan, Kansas 66506-2601

P. W. Schmidt
Department of Physics and Astronomy, University of Missouri, Columbia, Missouri 65221

T. P. Rieker
Center for Microengineered Materials, Department of Chemical and Nuclear Engineering, University of New Mexico, Albuquerque, New Mexico 87131

(Received 13 March 1998)

This paper studies the static structure factor of a system of fractal aggregates at various degrees of densification. The system we use for this study is carbonaceous soot, which is composed of diffusion limited cluster aggregates with a fractal dimension of 1.8. The range of density is great, from the aerosol to a system of lightly touching clusters and then to ground and compressed samples. The data involve a combination of light scattering and small-angle x-ray scattering over a q range of $3\times10^{-3}\leqslant q\leqslant 6\ \mathrm{nm}^{-1}$. We are able to explain all the features of the data with scaling arguments based on comparisons of the scattering length scale q^{-1}, where q is the magnitude of the scattering wave vector, and the various length scales of the system that are density dependent. [S1063-651X(98)00410-3]

PACS number(s): 61.10.Eq, 64.60.Ak, 61.43.Gt, 82.70.−y

I. INTRODUCTION

Many disordered solids are close assemblies of aggregates (clusters) of primary particles. Examples include wet gels, dried silica gels, and carbon blacks, all of which have important technological and scientific applications. The structure of these assemblies is an important factor in their physical properties. In the past, structural information has been obtained using small-angle x-ray scattering [1–3]. This method yields the structure factor $S(q)$, where q is the magnitude of the scattering wave vector, which is the spatial Fourier transform of the real space structure. Fourier inversion of the complete structure factor for these disordered solids is not possible due to their complexity, but a successful analysis has been achieved for various length scales and fractal dimensions characteristic of portions of the structure. At present, however, there is not a complete description covering all length scales of the structure factor for these systems.

Previous work on these assembled solids has built upon the knowledge of the structure factor for a single cluster by either piecing together structure factors with different length scales in an *ad hoc* fashion [4,5] or applying the single-cluster structure factor to the solid while ignoring intercluster effects [6–8]. However, the importance of intercluster correlations has been well demonstrated by experiments on aggregating colloids that display a peak in $S(q)$ when the clusters approach a point where they begin to fill all space, i.e., where they begin to gel [9–12]. This peak is due to intercluster correlations that develop some spatial coherency for nearly touching clusters not too polydisperse in size [13]. Hasmy *et al.* [14] recognized the importance of intercluster correlations for assembled solids through studies of computer simulated gels by studying both the correlation function $g(r)$ and structure factor $S(q)$. To determine $S(q)$, $g(r)-1$ was Fourier transformed. They subtracted unity from $g(r)$ to eliminate the effects of the macroscopic boundaries from $S(q)$; hence $S(q)\rightarrow 0$ as $q\rightarrow 0$. Forcing $S(q)$ to zero, however, creates a peak regardless of intercluster correlations and hence may mask or modify the effects of these correlations. Also, macroscopic boundaries exist in real systems and, as we shall see, play a significant role in the low-q regime of the structure factor.

The purpose of this paper is to provide a fundamental understanding of the structure factor of aggregate assemblies with multiple length scales. To gain this complete understanding we study the structure factor of a carbonaceous soot system as it evolves from the rarified aerosol to a compressed solid. Soot clusters have a fractal morphology with a fractal dimension of 1.8 indicative of formation by diffusion limited cluster-cluster aggregation. Our data will show how various length scales and slopes present in the structure factor evolve as the system evolves from the cluster-dilute aerosol phase, characterized by two length scales (cluster and primary particle size) and a mass fractal dimension, to a low-density solid wherein agglomerates of clusters form and intercluster separation becomes comparable to the cluster size, to a compressed solid wherein the mass fractility of the clusters is lost and the agglomerated assembly become a porous solid. Throughout this evolution, the primary particle size and morphology are invariant. Simple scaling arguments that we develop explain the evolution of the complete structure factor. We also show that the macroscopic boundaries cannot be neglected since they affect the experimental structure factor at low q through a Porod law rising from macroscopic surfaces.

II. EXPERIMENTAL METHODS

In this paper we study the structure factor of carbonaceous soot in five phases: (i) the aerosol phase in the flame, (ii) the ''fluffy'' solid phase accumulated on a metal plate

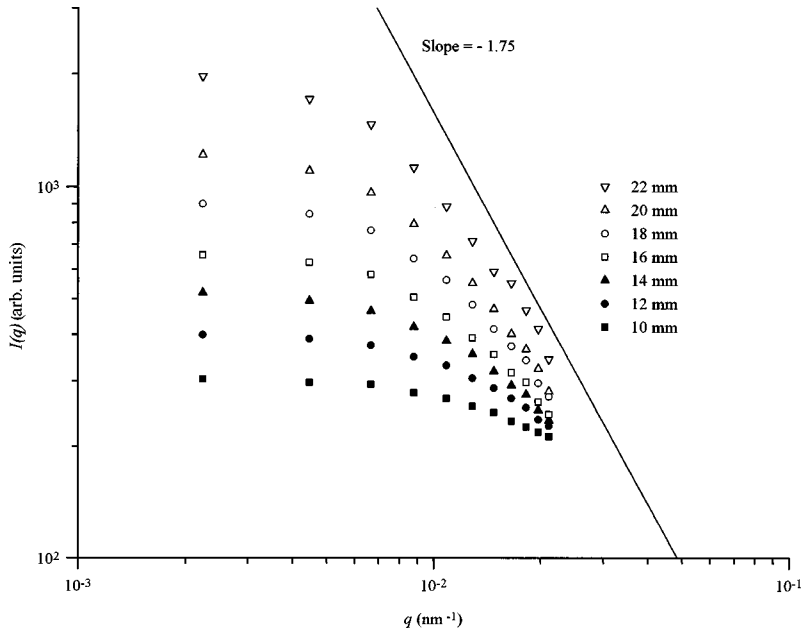

FIG. 1. Optical structure factor for soot aerosol in a premixed methane/oxygen flame with a carbon/oxygen ratio of 0.75 at various heights h above burner.

inserted into the flame, (iii) the ''ground'' phase, which is the fluffy phase ground in a mortar and pestle with moderate hand pressure for approximately 30 s, (iv) the ''fluffy compressed'' phase, which is the fluffy phase compressed under a pressure of 170 MPa, and (v) the ''ground compressed'' phase, which is the ground phase compressed under a pressure of 170 MPa.

The soot was produced in a premixed methane:oxygen flame with a C:O ratio of 0.75. The burner consisted of a cooled porous frit 6.0 cm in diameter, through which the combustible mixture passed at a flow rate of 200 cm^3/s. This frit was surrounded by an annular frit 0.5 cm wide, through which N_2 passed at a flow rate of 70 cm^3/s. The flame was stabilized by a 15-cm-diam stagnation plate 3.0 cm above the burner surface. This arrangement created an isolated, quasi-one-dimensional flame where the chief variable was the height above the burner.

The optical structure factor [15] measurement for the soot aerosol used an argon ion laser with $\lambda = 488$ nm as a light source. This involved measuring the relative scattered light intensity as a function of $q = 4\pi\lambda^{-1} \sin\theta/2$, the magnitude of the scattering wave vector at a scattering angle θ. The scattered light intensity was measured at a variety of angles ranging from 10° to 110°, as described previously [15,16]. This yielded a structure factor in the range $2.2\times10^{-3} \leqslant q \leqslant 2.1\times10^{-2}$ nm^{-1}.

Soot was collected on the stagnation plate. A layer of soot built up on this plate at a rate of about 0.2 mm/min. This is the fluffy sample. The density of this soot was determined to be 0.04 g/cm^3. The ground sample had a density of 0.17 g/cm^3. We were unable to measure the densities of the compressed samples. Small-angle x-ray scattering (SAXS) measurements were performed at the University of New Mexico/Sandia National Laboratories Small-Angle X-Ray Scattering Laboratory on the 5 Meter Pinhole (short geometry) and Bonse-Hart instruments [17].

III. RESULTS AND ANALYSIS

Figure 1 shows the optical structure factors of the soot aerosol phase measured with *in situ* light scattering. As height above burner increases, the aerosol has more time to aggregate and the clusters grow. This is evident in the fact that the bend in the structure factor curves goes to lower q to indicate larger clusters with increasing height. The large-q regime is approaching a slope of -1.8, which is consistent with the expected fractal dimension of soot clusters [18–20], which can be described by the diffusion limited cluster aggregation process [21,22].

Figure 2 shows the SAXS intensities as a function of q for the fluffy, ground, fluffy compressed, and ground compressed samples plotted double logarithmically. These are directly proportional to the structure factor $S(q)$. Both pinhole and Bonse-Hart data were combined to span a large-wave-vector range of $3\times10^{-3} \leqslant q \leqslant 6$ nm^{-1}. There are a number of important qualitative features visible in the figure. For $q \gtrsim 1$ nm^{-1} there is a q^{-2} regime due to scattering from graphitic sheets within the soot primary particles. For $1 \gtrsim q \gtrsim 10^{-1}$ nm^{-1}, the four samples show essentially the same behavior with $S(q) \sim q^{-4}$. We shall see that this regime is the Porod regime of the approximately spherical monomers that are the same in each sample. Interesting changes occur for $q \lesssim 10^{-1}$ nm^{-1}. The fluffy sample displays a relatively featureless curve in this regime that has an approximate slope of -1.8, the value expected for fractal aggregates of dimension $D = 1.8$. The denser ground sample is similar until $q \lesssim 7\times10^{-3}$ nm^{-1}, where it shows an upswing to a slope of approximately -4. In the denser, compressed samples this low-q, slope -4 regime becomes more pronounced while the intermediate, $7\times10^{-3} \leqslant q \leqslant 10^{-1}$ nm^{-1}, regime loses its fractal-like slope.

The behavior of the observed structure factors can be explained by scaling arguments involving the various length scales and quantities of the system. These arguments are

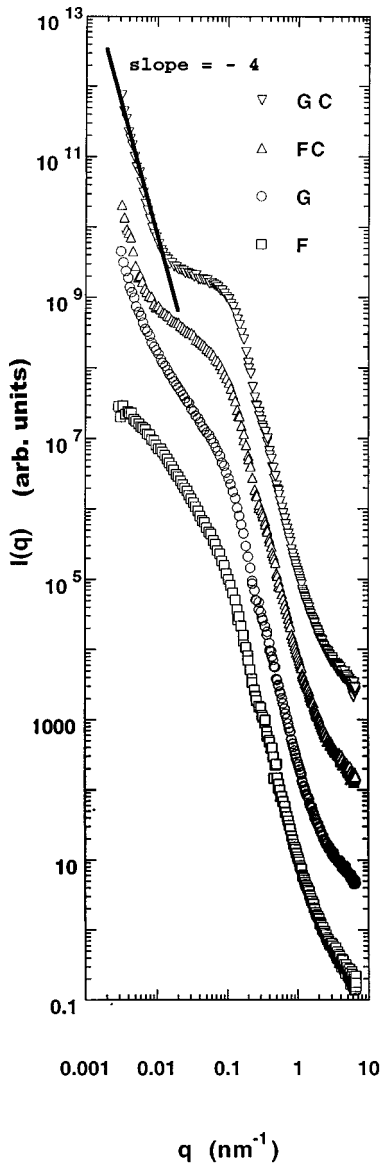

FIG. 2. SAXS structure factor (pinhole and Bonse-Hart data combined) for the four solid phases of soot: *F*, fluffy phase; *G*, ground phase; *FC*, fluffy compressed phase; *GC*, ground compressed phase. Each data set has been shifted upward by a factor of 15 relative to the set below it for clarity.

based on the numerical studies of Oh and Sorensen [23]. Figure 3 gives a schematic representation of the general form for the entire structure factor for the low-density, fluffy system, which we now explain. It also forms the basis to understand the high-density systems. The relevant length scales are L, a macroscopic length scale related to boundaries of the illuminated system, essentially the scattering volume size; R_{NN}, the mean, cluster nearest-neighbor, center to center separation; R_g, the cluster radius of gyration; and a, the primary particle or monomer radius. The lengths are all represented by their inverse on the q axis of the structure factor plot in Fig. 3. There are also three relevant quantities for describing the structure factor. They are N_m, the total number of monomers in the scattering volume; N_c, the total number of clusters in the scattering volume; and N, the average number of monomers in the cluster. These quantities

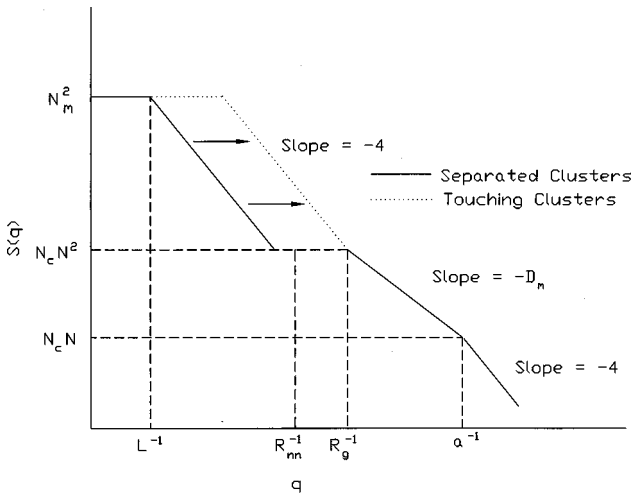

FIG. 3. Schematic diagram of the complete structure factor of a system of N_c clusters of primary particles of radius a, N primary particles per cluster, with a cluster radius of gyration R_g, and a cluster mass fractal dimension D_m. R_{nn} is the mean cluster-cluster nearest-neighbor separation in the system and L is the macroscopic system (scattering volume) size. There are $N_m = N_c N$ monomers in the system. The arrows show how the structure factor would be modified if the clusters were touching such that $R_{\mathrm{nn}} \rightarrow R_g$.

are related by $N_m = NN_c$. Our scaling argument relies on the inverse wave vector q^{-1}, which is the length scale of the experiment. When scattering occurs from points separated by distances greater than q^{-1}, the phases of the scattered waves differ greatly and randomly if the points are positioned randomly. Then the waves add incoherently so that the scattered intensity is proportional to the number of scattering points. If, on the other hand, the points all lie close relative to q^{-1}, the scattered waves are in phase regardless of the position of the points. Then the waves add coherently, so that the scattering amplitude is proportional to the number of points and hence the scattered intensity is proportional to the square of the number of points. With these concepts in mind, we begin our description at large q.

When $q > a^{-1}$, where $2a$ is the nearest-neighbor monomer spacing in a cluster, the monomer-monomer scattering is incoherent. Thus the scattering is proportional to N_m, independent of the state of aggregation. One may write

$$S(q) = N_m P(q), \tag{1}$$

where $P(q)$ is the form factor for the monomer particles. For example, for spherical particles with refractive index near unity, the Rayleigh-Debye-Gans formula would apply [24]. For $q < a^{-1}$, $P(q) = 1$, but for $q > a^{-1}$ the envelope of the form factor for a three-dimensional particle with a two-dimensional surface has a q^{-4} functionality called Porod's law. For modest monomer polydispersity the sharp minima in the form factor wash out to leave the q^{-4} functionality. Thus we expect

$$S(q > a^{-1}) = N_m q^{-4}, \tag{2}$$

which is plotted in Fig. 3 in the region $q > a^{-1}$.

It is well known that for mass fractal aggregates the q dependence in the regime $R_g^{-1} < q < a^{-1}$ is q^{-D_m} [3]. Here

we present a simple scaling argument for this result. Consider the points $(S(q),q)=(N_cN^2,R_g^{-1})$ and (N_m,a^{-1}) in Fig. 3. The first of these points results because when $q=R_g^{-1}$, all the N monomers within a single cluster are close relative to q^{-1} and hence they scatter coherently to yield the N^2 term; yet the inverse q is less than the cluster-cluster nearest-neighbor separation and hence the intercluster scattering is incoherent and thus proportional to the number of clusters N_c. The second point occurs from the logic of Eq. (2), i.e., that when $q=a^{-1}$ all the monomers scatter incoherently. Recall that $N_m=N_cN$ and use the fractal cluster scaling relation $N\sim(R_g/a)^{D_m}$. Then it follows that to link these two points one must have (on average)

$$S(R_g^{-1}<q<a^{-1})\sim q^{-D_m}. \tag{3}$$

At yet smaller q, consider the region $R_{\mathrm{NN}}^{-1}<q<R_g^{-1}$. In this region the scattering remains constant at N_cN^2 because, if the clusters are distributed uniformly, no new length scales are encountered. [Note that this uniform density of clusters is significantly different from the fractal distribution of monomers that led to a changing scattered intensity (3) in the previous regime.] Then

$$S(R_{\mathrm{NN}}^{-1}<q<R_g^{-1})=N_CN^2. \tag{4}$$

If cluster-cluster correlations exist, the constant behavior in Eq. (4) is broken near R_{NN}^{-1} [13]. Strong correlations yield a minimum at πR_{NN}^{-1} followed by a maximum at $2\pi R_{\mathrm{NN}}^{-1}$. Similar correlations between monomers in a cluster have been predicted and seen by Hasmy *et al.* [25]. A simple physical picture of the maximum follows from $2\pi R_{\mathrm{NN}}^{-1}=q=4\pi\lambda^{-1}\sin\theta/2\simeq 2\pi\lambda^{-1}\theta$, which yields $\theta\simeq\lambda/R_{\mathrm{NN}}$, a condition well known from Fraunhofer diffraction theory. Weaker correlations show a dip beginning near $1.5\pi R_{\mathrm{NN}}^{-1}$. Very weak or no cluster-cluster correlations leave $S(q)$ featureless and hence constant, as described by Eq. (4), near R_{NN}^{-1}.

Proceeding to yet smaller q, consider $L^{-1}<q<R_{\mathrm{NN}}^{-1}$. In this regime $q^{-1}>R_{\mathrm{NN}}$ implies that the system of clusters is unresolved by the scattering process, i.e., the individual clusters are not seen by the scattering process. Scattering from the system may arise from both fluctuations in the density of the clusters and from the edge, i.e., surface, of the entire illuminated system. For randomly distributed clusters the bulk, density fluctuation contribution will be small compared to the surface term. Thus the scattering can ''see'' only the macroscopic surface. This surface scattering is Porod scattering. We now present a scaling approach for Porod scattering. Imagine a volume of dimension L, the surface of which is tiled with cubes of side q^{-1} and hence volume q^{-3}. The number of scatterers or monomers within each surface cube is proportional to this volume and since they are within q^{-1} of each other, they scatter coherently. Thus the scattering per cube is proportional to the square of the cube volume q^{-6}. The total scattering from all the cubes on the surface is proportional to the number of cubes. In three dimensions the surface area scales as L^2. The number of cubes on this surface is L^2/q^{-2}. The total scattering is the product of the number of cubes times the scattering per cube $(L^2/q^{-2})(q^{-6})=L^2q^{-4}$. This is the Porod law in three-dimensional space. Because of the general nature of Porod's law demonstrated here and because L is the scattering volume size, we call the particular regime where $L^{-1}<q<R_{\mathrm{NN}}^{-1}$ the macroscopic scattering volume Porod regime and it is included in Fig. 3.

Finally, when $q<L^{-1}$, a region currently inaccessible to both SAXS and light scattering since $L\simeq 0.1$ mm, all the monomers in the entire system scatter coherently. Then

$$S(q<L^{-1})=N_m^2, \tag{5}$$

independent of the state of aggregation. This completes our description of the features in Fig. 3, which we now use to explain our scattering results.

Light scattering probes the region near $q\simeq R_g^{-1}$ for our clusters. The results for the aerosols in Fig. 1 show the general features depicted in Fig. 3 in this region. With increasing height above burner, the soot aerosol matures via aggregation to yield an increasing R_g and hence the structure factor passes from the flat Rayleigh regime with scattered intensity equal to N_CN^2 to the sloped, q^{-D_m} cluster fractal regime at larger q. This behavior has been well documented and measured by us and others in the past [15,16,26,27]. The wave vector magnitudes available with light are not large enough to achieve the end of this regime near $q\sim a^{-1}$. Moreover, we could not achieve scattering angles and hence q values small enough so that $q=R_{\mathrm{NN}}^{-1}$. Previous work on a similar flame indicates $R_{\mathrm{NN}}\sim 20\ \mu$m [28], which would require $\theta\sim 0.2°$ for $\lambda=488$ nm.

In the nonaerosol, solid soot samples the individual clusters are touching; thus we expect $R_{\mathrm{NN}}\simeq 2R$, where R is the perimeter radius approximately equal to $1.5R_g$ [see Eq. (7) below]. If this occurs, the structure factor in Fig. 3 would be modified as shown by the arrows. To understand the modification imagine the large volume aerosol with $R_{\mathrm{NN}}\gg R_g$ and then shrink the whole system until the clusters touch at $R_{\mathrm{NN}}\sim 3R_g$. The system size L must shrink by the same factor as R_{NN}. Hence the macroscopic Porod regime must uniformly slide over as indicated by the arrows in Fig. 3. Figure 3 shows that for a system of barely touching clusters the macroscopic, scattering volume Porod regime begins where the mass fractal regime of the individual clusters leaves off with declining q. This can be clearly seen in our data detailed in Fig. 4, where we plot the light scattering data for the aerosol and the SAXS data for both the fluffy and ground samples together.

This conclusion, that the fluffy sample is the aerosol sample shrunk until the clusters lightly touch, can be quantitatively supported by calculating the density of the fluffy sample. To obtain the size of the aggregates in the fluffy sample a Guinier analysis of the aerosol data at various heights above the burner was performed to determine R_g using [15,16]

$$S(q)\simeq S(0)(1-\tfrac{1}{3}q^2R_g^2) \tag{6}$$

and restricting the fit to $qR_g\leqslant 1$. R_g as a function height above the burner was extrapolated to $h=30$ mm, the height of the stagnation plate that collected the fluffy soot sample, to find $R_g\simeq 240$ nm. The perimeter radius R of the assumed spherical cluster is related to the radius of gyration by [29]

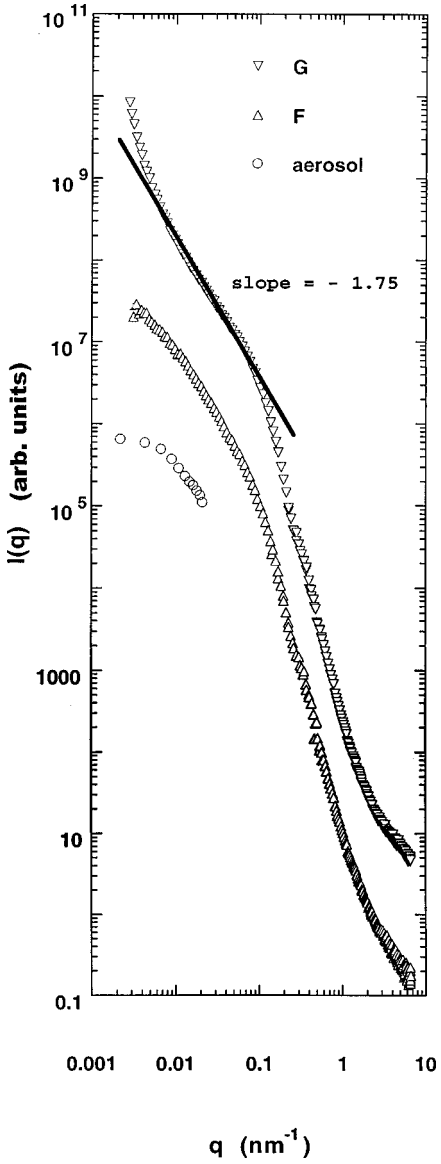

FIG. 4. Comparison of soot aerosol at a height above burner of 22 mm, fluffy sample (F) and ground sample (G) structure factors with arbitrary intensity scales.

$$R=[(D+2)/D]^{1/2}R_g. \tag{7}$$

To calculate the density of the fluffy sample we assume that these clusters are touching and the density of the carbon is 1.85 g/cm^3 and use

$$N=k_0(R_g/a)^D, \tag{8}$$

where $k_0=1.3$ as found in simulation [29,30] and experiment [31]. Then, for a monomer size of $a=18$ nm (see below) the density is calculated to be 0.035 g/cm^3. This semiquantitative calculation yields good agreement with the measured density of 0.04 g/cm^3.

This calculation implies that the mean cluster separation in the fluffy sample is $R_{\mathrm{NN}}\simeq 2R\simeq 700$ nm, which we determined by using Eq. (7), $R_g\simeq 240$ nm, and $D=1.8$. Thus the macroscopic Porod regime for the fluffy soot should begin near $q^{-1}=R_{\mathrm{NN}}\sim 1.4\times 10^{-3}$ nm^{-1}, which is just below our q range. Indeed, Fig. 4 shows no macroscopic Porod regime

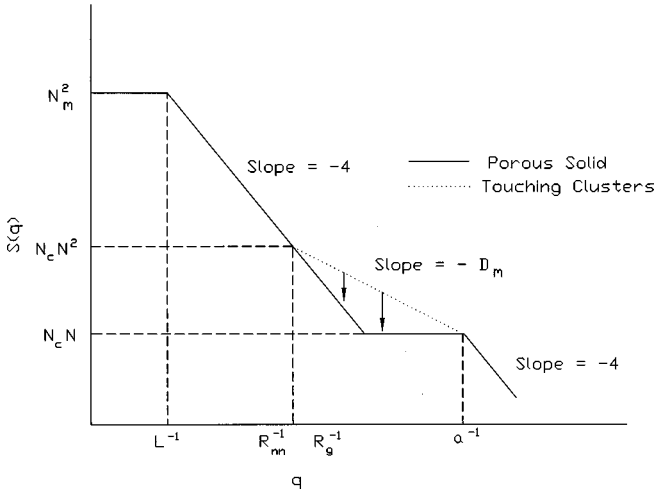

FIG. 5. Schematic diagram of a porous solid created by compressing agglomerates of clusters composed of spherical monomers of radius a. There are N_m monomers in the system defined by the scattering volume size L. Arrows indicate how the mass fractal regime of the N_c clusters with N monomers per cluster is altered by the compression.

for the fluffy soot. It does show increasing positive deviation of the fluffy soot scattered intensity relative to the aerosol and this is most likely a combination of the precursor to the upswing expected and the fact that R_g for the fluffy soot is larger than in the aerosol at $h=22$ mm.

We can reverse the argument above to calculate R_{NN} for the ground sample from its measured density of 0.17 g/cm^3. This yields $R_{\mathrm{NN}}\simeq 200$ nm. Hence the macroscopic Porod regime should begin near $q\simeq R_{\mathrm{NN}}^{-1}\simeq 5\times 10^{-3}$ nm^{-1}, which is consistent with the ground soot structure factor in Fig. 4. An alternate way of describing the low-q, q^{-4} regime is to make use of the fact that $q^{-1}>R_{\mathrm{NN}}$ in this regime. Thus the scattering is seeing more than one cluster in a coherence region, i.e., it is seeing an agglomeration of clusters. This is true regardless of whether the clusters are in fact touching in the agglomerate, as in the fluffy sample, or not, as in the aerosol sample. In this latter case we generalize the concept of agglomerate to mean any ensemble of entities, touching or not, spread uniformly through space. For any agglomerate of uniformly distributed mass, scattering occurs from the surface of the agglomerate and hence, in analogy to scattering from a uniform sphere and consistent with our scaling argument above, Porod scattering, q^{-4}, follows.

In summary, the large upswing or increase in intensity at low q as the system densifies from aerosol to fluffy to ground sample is due to the decreasing value of R_{NN} whose inverse marks the beginning of the scattering volume Porod regime. This macroscopic scattering volume may be viewed as an agglomerate of clusters with agglomerate size L, the scattering volume size. The only structural implication of this low-q regime is that the scatterers are distributed uniformly over length scales greater than R_{NN}.

To explain the compressed soot samples consider that with compression we expect that certainly the outer regions and, with sufficient compression, the inner regions of the individual clusters will be destroyed. This means the length scales R_g and R_{NN} will be obliterated, but the monomer size

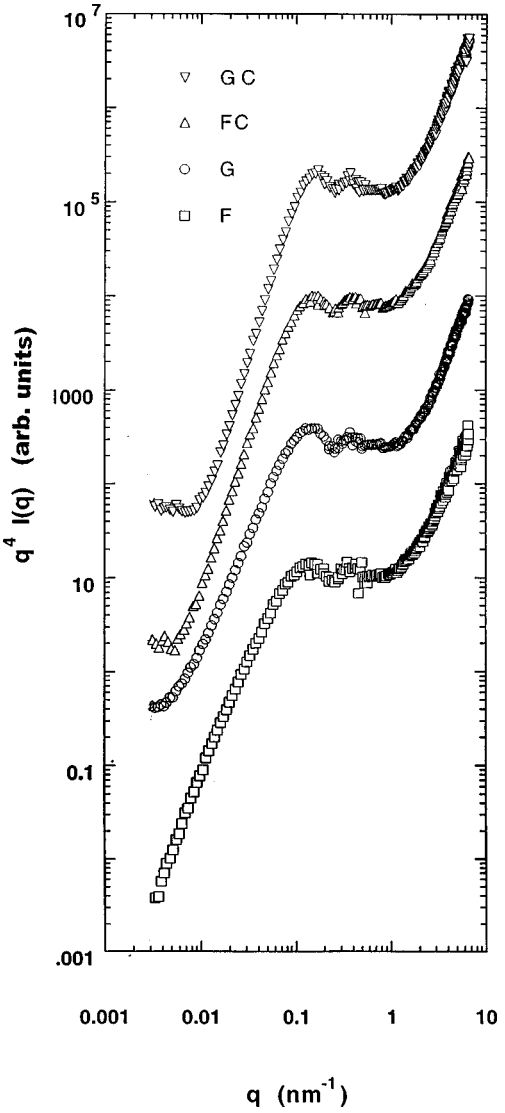

FIG. 6. SAXS structure factor data multiplied by q^4 vs q, where q is the scattering wave vector for the fluffy (F); ground (G); fluffy compressed (FC); and ground compressed (GC) phases.

will remain the same in all except the most extreme compression. Thus the cluster mass fractal regime in the structure factor should not be present and the structure factor should show no structure at the length scales R_g and R_{NN}. Both these predictions are consistent with the data in Fig. 2. What replaces the agglomeration of fractal clusters is a porous solid with an upper length scale of L and a lower length scale related to the pore size, with uniform density on scales between these limits. Thus Porod scattering is again obtained with $S(q)\sim q^{-4}$ beginning at L^{-1} and dropping uniformly until q^{-1} becomes commensurate with the pore size. Thereafter, the structure factor shows no q dependence until the monomer length scale is achieved [23]. This behavior is shown schematically in Fig. 5 and it reproduces the experimental results in Fig. 2 well. Note that the length scales R_{NN} and R_g have been obliterated by the compression. The monomer, however, is unaffected; thus the structure factors overlap for $q\gtrsim a^{-1}$.

The knee in the SAXS data near $q\simeq 10^{-1}$ nm^{-1} is due to the monomer size. To facilitate analysis in this regime and to

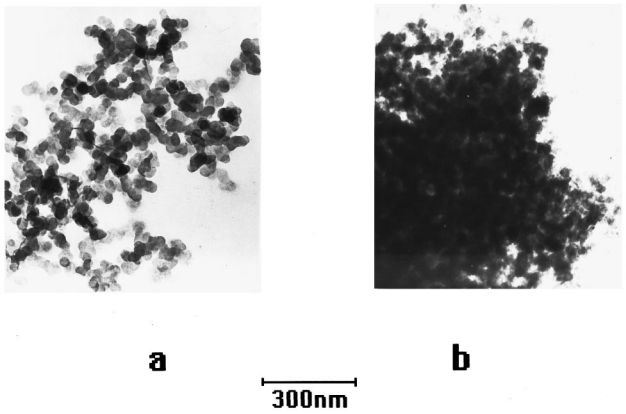

FIG. 7. TEM photograph of (a) fluffy soot sample and (b) ground compressed soot sample.

make the monomer scattering in the region $q\gtrsim 10^{-1}$ nm^{-1} more apparent, we replot the data of Fig. 2 in Fig. 6 as $q^4I(q)$ vs q. Qualitative inspection of Fig. 6 shows that all samples display essentially the same monomer scattering with apparently the same monomer size. This graph also shows vague interference ripples for $1\gtrsim q\gtrsim 10^{-1}$ nm^{-1}. A monodisperse system of spherical particles would yield highly visible interference ripples. Thus the fact that these ripples are not completely washed out implies that the soot monomers do not deviate very far from sphericity and are not very polydisperse. Also note that the graph does a good job of highlighting the length scales near $q\simeq 10^{-2}$ nm^{-1}, which we discussed above as due to overall cluster size and separation and the impending, at lower q, scattering volume Porod regime.

Quantitative fits to this regime were obtained by using the Rayleigh-Gans-Debye form factor for spheres [24],

$$P(q)=[3(\sin qa-qa\cos qa)/(qa)^3]^2. \tag{9}$$

This form factor was convolved with a Gaussian distribution, to account for polydispersity of the monomer radius [25], given by (unnormalized) [32,33]

$$\overline{P(q,a_0)}=\int_0^\infty P(q,a)\exp[-(a-a_0)^2/2\sigma^2]da. \tag{10}$$

Scattering curves were calculated for various values of the mean a_0 and standard deviation σ and compared to the data. The best match to the data was for $a_0=17.5$ nm and $\sigma=3$ nm ($\sigma/a_0=17\%$ polydispersity).

These results can be compared to TEM inspection of the soot samples. Figure 7 shows both the fluffy and ground compressed samples. The mean monomer radius was determined to be 18 ± 4 nm, in excellent agreement with the scattering results. The overall visual appearance is consistent with the scattering interpretation that the fluffy sample has more open space than the ground compressed sample.

IV. CONCLUSIONS

The scaling arguments that we have presented are successful in accounting for the general features of the structure factor of a system of fractal clusters as their mean separation

evolves from large to small and when, in the small separation limit, their fractal nature is destroyed by compression. The scaling argument was based on comparing the length scale of the scattering experiment q^{-1} to the length scales in the system and the notion that when scattering emanates from regions closer than q^{-1}, the scattering is coherent and thus proportional to the number of scattering entities squared, and when scattering emanates from regions farther apart than q^{-1}, the scattering is incoherent and hence linearly proportional to the number of scattering entities. The scaling argument successfully predicts scattering magnitudes and power law dependences, but cannot yield the form of the crossovers at the various length scales.

ACKNOWLEDGMENTS

We thank Paul Hubbard for technical assistance. The work at Kansas State University was supported by the NSF under Grants Nos. CTS-9408153 and CTS-9709764. T.P.R. acknowledges support from Sandia National Laboratories, operated for the U.S. Department of Energy under Contract No. DE-AC04-98A185000.

[1] A. Guinier, G. Fournet, C. B. Walker, and K. L. Yudowitch, *Small Angle Scattering of X-Rays* (Wiley, New York, 1955).
[2] *Small-Angle X-Ray Scattering*, edited by O. Glatter and O. Kratky (Academic, New York, 1982).
[3] P. W. Schmidt, in *Modern Aspects of Small-Angle Scattering*, edited by H. Brumberger (Kluwer, Dordrecht, 1995), p. 1.
[4] G. Beaucage, J. Appl. Crystallogr. **28**, 717 (1995).
[5] G. Beaucage and D. W. Schaefer, J. Non-Cryst. Solids **172-174**, 797 (1994).
[6] T. Freltoft, J. K. Kjems, and S. Sinha, Phys. Rev. B **33**, 269 (1986).
[7] G. Dietler, C. Aubert, D. S. Cannell, and P. Wiltzius, Phys. Rev. Lett. **57**, 3117 (1986).
[8] B. Cabane, M. Dubois, F. Lefaucheux, and M. C. Robert, J. Non-Cryst. Solids **119**, 121 (1990).
[9] M. Carpineti and M. Giglio, Phys. Rev. Lett. **68**, 3327 (1992).
[10] J. Bibette, T. G. Manson, H. Gang, and D. A. Weitz, Phys. Rev. Lett. **69**, 981 (1992).
[11] M. Carpineti and M. Giglio, Phys. Rev. Lett. **70**, 3828 (1993).
[12] D. J. Robinson and J. C. Earnshaw, Phys. Rev. Lett. **71**, 715 (1993).
[13] H. Huang, C. Oh, and C. M. Sorensen, Phys. Rev. E **57**, 875 (1998).
[14] H. Hasmy, E. Anglaret, M. Foret, J. Pelous, and R. Jullien, Phys. Rev. B **50**, 6006 (1994).
[15] S. Gangopadhyay, I. Elminyawi, and C. M. Sorensen, Appl. Opt. **30**, 4859 (1991).
[16] C. M. Sorensen, J. Cai, and N. Lu, Appl. Opt. **31**, 6547 (1992).
[17] T. P. Rieker and P. F. Hubbard, Rev. Sci. Instrum. (to be published).
[18] S. R. Forrest and T. A. Witten, Jr., J. Phys. A **12**, L109 (1979).
[19] R. J. Samson, G. W. Mulholland, and J. W. Gentry, Langmuir **3**, 273 (1987).
[20] C. M. Sorensen and G. D. Feke, Aerosol. Sci. Technol. **25**, 328 (1996).
[21] M. Kolb, R. Botet, and R. Jullien, Phys. Rev. Lett. **51**, 1123 (1983).
[22] P. Meakin, Phys. Rev. Lett. **51**, 1119 (1983).
[23] C. Oh and C. M. Sorensen (unpublished).
[24] M. Kerker, *The Scattering of Light and Other Electromagnetic Radiation* (Academic, New York, 1969).
[25] A. Hasmey, M. Fouet, J. Pelous, and R. J. Jullien, Phys. Rev. B **48**, 9345 (1993).
[26] H. X. Zhang, C. M. Sorensen, E. R. Ramer, B. J. Olivier, and J. F. Merklin, Langmuir **4**, 867 (1988).
[27] U. O. Köylü and G. M. Faeth, Heat Transfer **116**, 971 (1994).
[28] C. Oh and C. M. Sorensen, J. Aerosol Sci. **28**, 937 (1997).
[29] C. Oh and C. M. Sorensen, J. Colloid Interface Sci. **193**, 17 (1997).
[30] C. M. Sorensen and G. C. Roberts, J. Colloid Interface Sci. **186**, 447 (1997).
[31] J. Cai, N. Lu, and C. M. Sorensen, J. Colloid Interface Sci. **171**, 470 (1995).
[32] P. W. Schmidt and M. Kalliat, J. Appl. Crystallogr. **17**, 27 (1984).
[33] T. P. Ricker, A. Hanprasopwattana, A. Datye, and P. Hubbard (unpublished).